



Temperature and curvature insensitive all-fiber sensor used for human breath monitoring

WEIHAO YUAN,¹  LINGDUO LI,² YU WANG,^{1,*}  ZHENGANG LIAN,³  DARU CHEN,⁴ CHANGYUAN YU,¹  AND CHAO LU¹

¹Photonic Research Centre, Department of Electronic and Information Engineering, The Hong Kong Polytechnic University, Hong Kong, China

²Photonics Research Centre, Shenzhen Research Institute of The Hong Kong Polytechnic University, Shenzhen, China

³Yangtze Optical Electronics Co., Ltd. (YOEC), Fifth Hi-Tech Avenue, East Lake Hi-Tech Development Zone, Wuhan 430205, China

⁴Hangzhou Institute of Advanced Studies, Zhejiang Normal University, Hangzhou 311231, China

*yuldy.wang@connect.polyu.hk

Abstract: In this paper, an all-fiber sensor based on hollow core Bragg fiber (HCBF) is proposed and successfully manufactured, which can be used for human breath monitoring. Benefiting from the identical outer diameters of HCBF and single mode fibers (SMFs), the sensor can be directly constructed by sandwiching a segment of HCBF between two SMFs. Based on optical propagation properties of HCBF, the transmission light is sensitive to specific environmental change induced by human breath. Thus, the breath signals can be explicitly recorded by measuring the intensity of the transmitted laser. The sensor presents a rapid response time of ~ 0.15 s and recovery time of ~ 0.65 s. In addition, the HCBF-based sensor shows good insensitivity to the variation of temperature and curvature, which enables its reliable sensing performance in the dynamic and changeable environment.

© 2021 Optical Society of America under the terms of the [OSA Open Access Publishing Agreement](#)

1. Introduction

Optical fiber sensors have attracted wide attention because of advantages such as cost-efficient manufacture, ease of fabrication, outstanding electromagnetic and chemical resistance, etc. Various fiber sensors have been investigated for widespread applications, including temperature [1,2], humidity [3,4], curvature [5–7], refractive index (RI) [8,9], gas [10,11], pH value [12] and vital signs monitoring [13]. The vital signs monitoring, including human breath and heartbeat detection, is a promising research direction for fiber sensors. Human breath plays an important role in the noninvasive diagnosis of diseases. The health status of people can be evaluated by breath frequency and depth which entails the sensor with the capability of continuous monitoring and fast response time. To date, a variety of specialized optical fiber structures have been developed for human breath monitoring. In 2010, Akita et al. developed a hetero-core optical fiber structure coated with hygroscopic polymer layers, which can be used for human breath monitoring, and the response time reached 400 ms [14]. After that, in 2017, Li et al. reported the side polished optical fiber coated by molybdenum disulfide with the response time of 0.85 s and the recovery time of 0.85 s [15]. In 2018, Aldaba et al. proposed the sensor based on SnO₂ sputtering deposition on a microstructured optical fiber Fabry-Pérot (FP) sensing head that shows a response time of 370 ms and a recovery time of 380 ms [16]. Afterward, Jiang et al. demonstrated a fiber sensor by depositing graphene oxide onto tilted fiber grating, exhibiting an ultrafast response within ~ 42 ms [17]. In 2020, Li et al. proposed a gelatin film assisted fiber breath sensor consisting of a microknot resonator superimposed on a Mach-Zehnder interferometer with an ultrafast response of 84 ms and recovery time of 29 ms [18]. However, all

the fiber sensors used for human breath monitoring are combined with materials that may limit their applications in various ambient.

In view of this, to overcome the inconvenience brought by materials, we firstly propose and experimentally demonstrate an all-fiber sensor based on hollow core Bragg fiber (HCBF) used for human breath monitoring. Many HCBF-based sensors have been investigated before which demonstrates the excellent performances in sensing applications [19–21]. The sensor presented in this work is composed of 2.5 cm-length HCBF, which is directly spliced between two pieces of single mode fibers (SMFs). Due to human breath induced cladding modes dissipation of HCBF, the breath signals can be demodulated by the variation of light transmission intensity. Unlike the materials-assisted fiber sensors, the fiber sensor proposed in this work is of all-fiber structure. It should be noted that materials-assisted fiber sensors may have a severe problem with sensor instability which can be caused by materials alteration or loose combination due to temperature change or chemical corrosion. Herein, we proposed an all-fiber sensor to solve the aforementioned problems. The HCBF-based sensor shows a fast response time of 0.15 s and recovery time of 0.65 s. In addition, the test of the proposed sensor at different temperature and curvature values is conducted. The experimental results demonstrate that the sensor is insensitive to the variation of temperature and curvature. Moreover, benefiting from the all-fiber structure, the stability of the sensor can be guaranteed due to the properties of optical fibers with intensely structural stability and chemical resistance.

2. Design and fabrication of the HCBF-based sensor

The hollow core Bragg fiber is a kind of hollow core photonic crystal fibers (HC-PCFs) in which light is guided in the air core confined by the photonic bandgap cladding. In most of the proposed works, the cladding of the HC-PCFs is a periodic arrangement of air holes running along the entire length of the fiber. Different from these fibers, HCBF confines light in the air core surrounded by one-dimensional rings with low and high refractive index functions as Bragg reflector but not two-dimensional lattice holes. With the increase of the pairs of bilayers, the transmission loss decreases, and most of the guided energy will be confined and guided in the air core, which is beneficial to high-power light delivery. However, in some sensing applications, part of the guided light is expected to spread out of the cladding and interact with the external environment to detect specific parameters with high sensitivity effectively. According to our previous simulation result and fiber drawing experience [22], four pairs of bilayers and a large air core with the diameter of 32 μm is an optimized tradeoff. In order to match with link fiber, the 125 μm outer diameter of the HCBF is the same as the outer diameter of a SMF. The cross-section view of the proposed HCBF is photographed by scanning electron microscope (SEM) and the refractive index distribution is shown in Fig. 1.

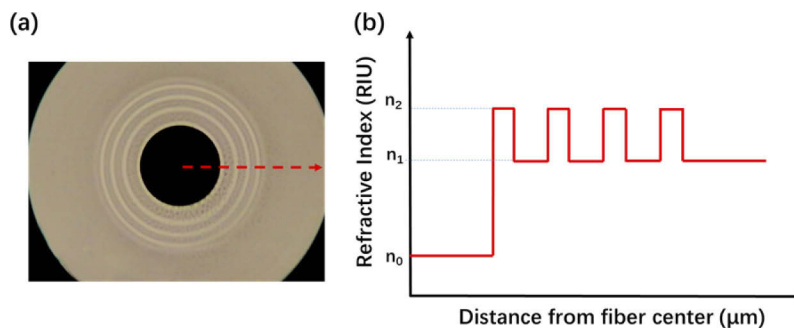


Fig. 1. (a) The cross-section view of HCBF and (b) refractive index distribution along the radial direction

The preform of the Bragg fiber was deposited in the inner side of a commercial silica tube by using a modified chemical vapor deposition (MCVD) equipment and drawn into expected fiber via a modified drawing tower [23]. The high and low refractive index (RI) at 1550 nm and the thickness of each layer are 1.454, 1.444, 1.06 μm , and 3.07 μm , respectively. It is noted that the fiber is fabricated through optical fiber preform melting at high temperature (1900 $^{\circ}\text{C}$). The Ge ions doped in the core area are hard to diffuse to cladding area even at 1900 $^{\circ}\text{C}$. After the annealing process, the produced fiber structure can have extreme stability.

The schematic diagram of HCBF-based sensor and the microscope image of the splicing point between HCBF and SMF are shown in Figs. 2(a) and 2(b). Due to the identical diameters of HCBF and SMF, the HCBF can be manually spliced with SMF without size mismatch. A commercial fusion splicer (FITEL, S178A, FURUKAWA) is used in the experiment. The discharge amount is chosen as the value of 20 shown in the device and the arc duration is 200 ms. The arc power and duration time have been optimized to minimize the deformation of the air core and ensure the mechanical strength of the splicing points. As can be seen from Fig. 2(a), the HCBF-based sensor is composed of HCBF sandwiched between two pieces of SMFs. Based on the results of our previous studies [22], the applied length of HCBF is chosen as 2.5 cm, which can ensure a relatively large transmission intensity and the coverage of human breath area. The light can be coupled into HCBF through lead-in SMF and collected by the other for data recording and analysis.

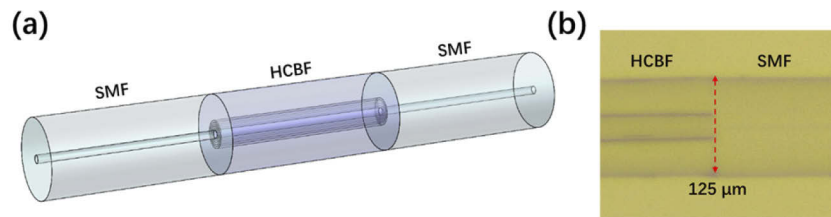


Fig. 2. (a) The schematic diagram of HCBF-based sensor and (b) the microscope image of splicing point between HCBF and SMF

The guiding mechanism of the HCBF is presented in Fig. 3. Referring to Fig. 1(b), the effective refractive index of the air and the cladding are n_0 and n_e (approximately equals to n_1), respectively. With the limited light confining ability of the only four bilayers, the light guided in the core can partially leak out of the Bragg rings, and be reflected from the outer surface of the cladding back into the fiber core. This can be explained using the anti-resonant reflecting optical waveguide (ARROW) theory, and the cladding of the HCBF can be regarded as an FP etalon. According to the ARROW model, the light at the anti-resonant wavelength tends to spread out of the cladding that will result in a loss dip in the transmission spectrum. The anti-resonant wavelength can be expressed as

$$\lambda_m = \frac{2d}{m} \sqrt{n_e^2 - n_0^2} \quad (1)$$

where m is an integer, n_e represents the effective refractive index of the cladding and d is the thickness of the cladding. The wavelength far away from the anti-resonant wavelength is called the guided band of HCBF, where the transmission loss is much lower. It is noted that the light intensity guided through the fiber at the guided band depends on the photonic bandgap effect of the Bragg bilayers and the reflectivity of the outer surface. When the reflectivity of the outer surface decreased under specific conditions, the transmission loss in the guided band will become higher.

Human breath contains a certain amount of water. When it reaches the HCBF-based sensor, this moisture condenses on the outer surface will form an uneven water film, which will destroy

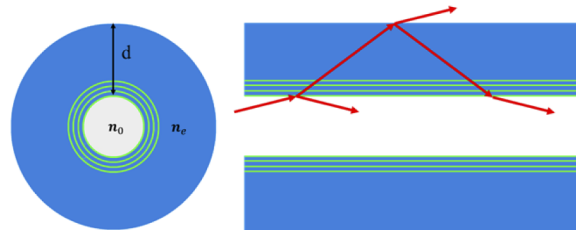


Fig. 3. The schematic diagram of the guiding mechanism of the HCBF

the uniform silica reflecting surface and increase the transmission loss at the guided band. Thus, based on the mechanism, the HCBF sensor can be applied for human breath monitoring by detecting the variation of the transmission intensity in the guided band. In the human breath monitoring experiment, a single frequency laser within the guided band was launched into the fiber, and the transmission light intensity will rise and fall as the breathing progresses.

We have tested the transmission spectrum of the HCBF with length of 7 mm to study the characteristics of the HCBF, as shown in Fig. 4(a). Several loss dips in the spectrum are consistent with theoretical analysis based on the ARROW theory. Some ripples in the transmission spectra are caused by the multiple reflections of the guided light on the inner and outer surfaces of the fiber cladding and the multiple-mode interference. At the wavelength far away from the anti-resonant dips, the loss is obviously lower, which is beneficial from the ARROW mechanism of the cylindrical HCBF and the photonic bandgap effect of the four Bragg bilayers. According to our previous work [22], the minimum loss of the HCBF in the guided band is much lower than that of the hollow core capillary (HCC) with the same size as our fiber. In order to testify the advantages of the Bragg structure, the contrast experiment was carried out. The HCC with inner/outer diameters of 25/125 μm was chosen to form the same structure, and the transmission spectra are illustrated in Fig. 4(b). The ripples in the transmission spectra of the HCBF are much slighter than those in HCC, because more light is confined in the core and less involved in the multiple reflections in the guided band. The flat and smooth guided band in our human breath monitoring experiment is highly advantageous because it can maintain the stability of the transmission light intensity even if the transmission spectrum redshifts/blueshifts with temperature or curvature fluctuation.

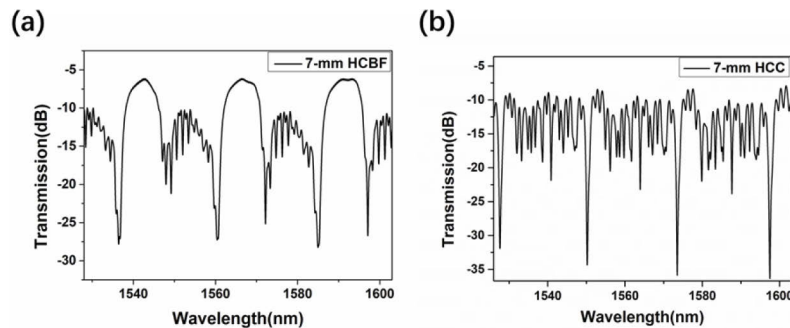


Fig. 4. The transmission spectra of the (a) HCBF and (b) HCC with both lengths of 7 mm

3. Experiment on human breath monitoring

The schematic diagram of experimental setups is displayed in Fig. 5. The broadband light source (BBS) has a bandwidth from 1528 nm to 1603 nm with a fixed optical power of 10 mW. The tunable laser (TL) can be tuned from 1480 nm to 1640 nm with a power range of 0–50 mW. The optical spectrum analyzer (OSA, YOKOGAWA, AQ6374) with the bandwidth of

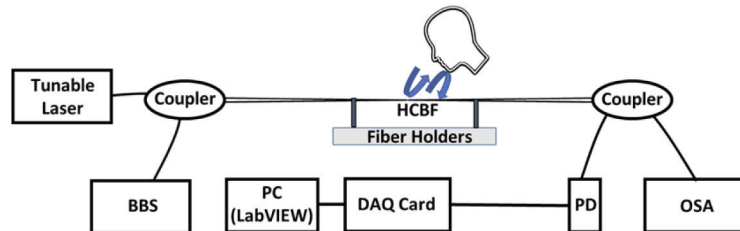


Fig. 5. The schematic diagram of experimental setups

350–1750 nm and resolution of 0.05 nm is used for recording transmission spectra. The photodiode (PD) with 3 dB bandwidth of 3 GHz and Data Acquisition (DAQ) Card with the data acquisition rate of 100 K are employed for electrical signal collection. The optical paths can be divided into two parts: BBS and OSA are applied to analyze optical spectra; TL and PD are used for electrical signal acquisition. The light emitted from BBS and TL can be coupled into HCBF sensor and received by OSA and PD, respectively. The electrical signals from PD are collected by DAQ card, which is controlled by LabVIEW on Personal Computer (PC). The collection rate of 1000 Hz and sampling points of 50176 are applied for human breath data collection.

The transmission spectra of HCBF-based sensor are displayed in Fig. 6(a). The optical spectrum is collected from 1528 nm to 1603 nm with the resolution of 0.05 nm, and it is seen that three peaks are observed in the measurement range. The red line in Fig. 6(a) represents the transmission spectrum under the status of no breath at room temperature (RT, 23–25 °C), and the blue line shows that in the status of breathing. Obviously, the decrease of peak value at around 1543 nm can be observed when human breathe towards the fiber sensor, which can be attributed to the cladding modes depletion caused by fiber-surface moisture-content change. Thus, the HCBF-based all-fiber sensor can be applied for human breath monitoring based on optical amplitude detection. In addition, it can be observed that there is a slight difference of transmission intensity at the third peak in Fig. 6(a) between breath and no breath, which is due to the recovery of moisture-content condition on the fiber surface. As seen from Fig. 6(b), the electrical signals of experimental results on human breath monitoring are presented that the black line indicates the collected signals without breath and the red line represents that with human breath. The TL at 1543 nm with a power of 1 mW is utilized as the light source. The laser will transmit through the HCBF and be collected by the PD and DAQ card controlled by LabVIEW. It can be observed that breath signals are explicitly revealed with 14 times breathing in 50 s and breath interval of around 3.5 s, according with results recorded through human-eye observation.

To analyze the relationship between breath and electrical signals, the experiment of one deep expiration was conducted, which is shown in Fig. 7. As generally known, a breathing process can be split into inspiration and expiration, and it is readily comprehensible that inspiration makes a slight impact on moisture change. As the human breath monitoring in this work is based on moisture-content detection, inspiration can be seemed as the recovery process of breath sensing. Expiration has a powerful influence on moisture around the fiber sensor so that the experimenter kept one deep expiration (lasting for around 6 s) towards the sensor for the signal catch. As can be seen from Fig. 7, the signal declines rapidly in the first 2 s, which can be explained by the decrease of light transmission due to moisture rising induced cladding modes dissipation. In this

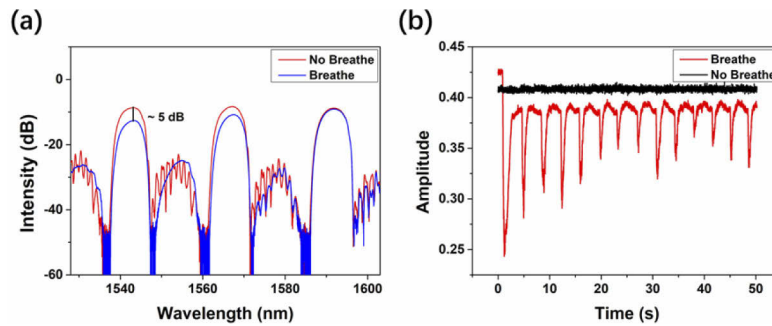


Fig. 6. (a) The transmission spectra of fiber sensor without breath (red line) and with breath (blue line) and (b) electrical signals without breath (black line) and with breath (red line)

process, the moisture increasing caused by expiration is stronger than moisture decreasing caused by evaporation of water molecules. In 2–6 s, although the experimenter continues expiration, the signal is reversely enhanced, which can be interpreted that the evaporation process becomes dominant.

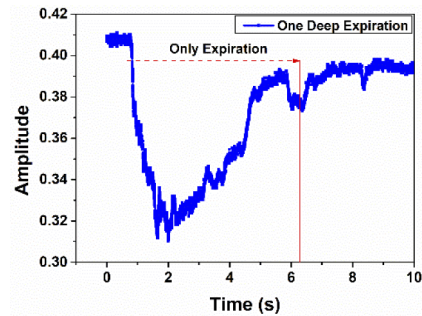


Fig. 7. Breath signal with one deep expiration

In addition, the distance between the human face and fiber sensor is studied to investigate its influence on sensing performance. As can be seen from Fig. 8(a), different distances of 2 cm, 5 cm, 10 cm are set for data recording. The blue line represents the breath signals detected at the distance of 2 cm, and the red line shows the sensing results at 5-cm distance. It is clear that

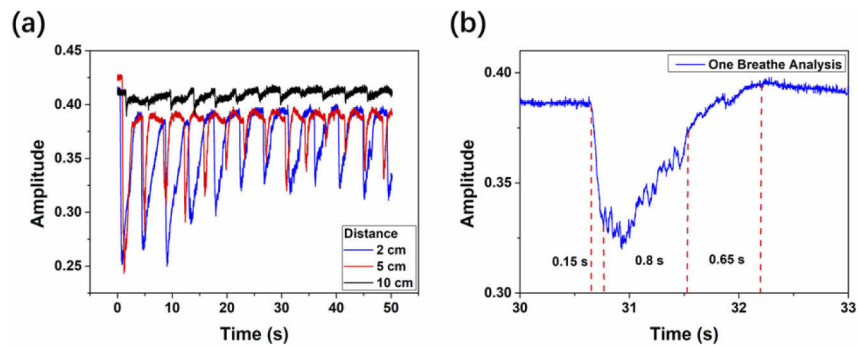


Fig. 8. (a) Electrical signals with different distances between the human face and fiber sensor at 2 cm, 5 cm, and 10 cm and (b) response time of human breath monitoring

there are slight differences between the two sets of signals. However, as the distance is increased to 10 cm, the amplitude of breath signals declined remarkably, which is shown as the black line. Although the 10-cm breath signals can still be distinguished, the weak amplitude will lead to measurement errors with a high probability. Considering this, the effective distance of the HCBF-based sensor used for human breath monitoring is less than 10 cm. Figure 8(b) shows the response time of the fiber sensor. Based on the data analysis in Fig. 7, the one breath signal can be divided into three parts. The ~ 0.15 s time slot represents the rapid-declining process of signal amplitude induced by human expiration. Then the amplitude of the signal fluctuates and recovers in the next ~ 0.8 s until the end of the expiration process. After that, the sensor is completely recovered in the next ~ 0.65 s within the process of human inspiration. Thus, the response time of the fiber sensor is measured to be around 0.15 s.

4. Test on temperature and curvature sensitivity

For all-fiber sensor used for human breath monitoring, the temperature and curvature will be the nonnegligible factors which may lead to significant measurement errors on sensing results. In view of this, further experiments are conducted to investigate the potential impacts of temperature and curvature on the proposed sensor structure. The fiber sensor was located in the temperature chamber with a resolution of 0.1 °C for temperature sensing. The BBS and OSA served as the light source and spectra recorder, respectively.

Figure 9(a) displays the transmission spectra of HCBF-based sensor at different temperatures of 25 °C, 30 °C, 35 °C, 40 °C, 45 °C, 50 °C. Evidently, the transmission spectra at different temperatures approximately maintain the same waveshapes but with a slight redshift. It is distinct that the light intensity at 1543 nm, which is the applied wavelength of TL for breath signal recording, is almost unchanged. The fluctuation of peak values keeps within 0.17 dB in the temperature range of 25–50 °C, as shown in Fig. 9(b), which is negligible compared to the 5 dB variation induced by human breath. Hence, the proposed all-fiber sensor used for human breath monitoring can be considered as temperature insensitive. In addition, the sensor can also be used for temperature sensing based on the wavelength shift, which is induced by the difference of RI change between Ge-doped high-index layers and low-index layers. Figure 9(c) presents the relationship between temperature change and wavelength variation at the interference dip of 1550 nm. The sensitivity is measured to be 16.5 pm/°C with the adjusted R-square value of 0.9983.

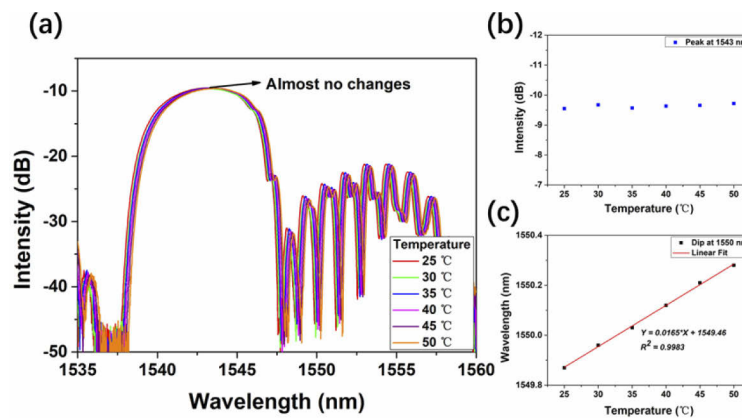


Fig. 9. (a) The details of transmission spectra at different temperatures of 25 °C, 30 °C, 35 °C, 40 °C, 45 °C, 50 °C, (b) the peak intensities statistics at different temperatures and (c) the relationship between temperature and dip (1550 nm) wavelength

As shown in Fig. 10, the experiment on curvature sensing can be conducted by fixing the fiber sensor on two translation stages (one is fixed, and the other one is moveable). By tuning the moveable translation station with a step of 20 μm , different curvature values can be achieved. In general, the curvature can be calculated by the equation shown below [24]:

$$c = \frac{1}{R} \cong \sqrt{\frac{24x}{L_0^3}} \quad (2)$$

where C represents the curvature value, R refers to the bending radius, x is the displacement of the moveable stage, and L_0 (8.5 cm) is the fiber length between two fiber holders when the fiber is straight.

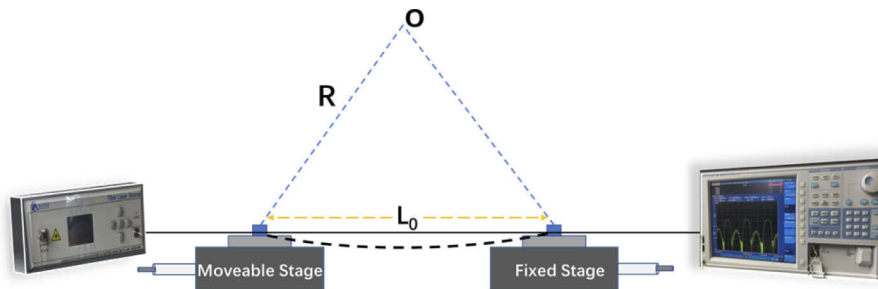


Fig. 10. The schematic diagram of the experimental setup for curvature sensing

The experimental results of curvature sensing are presented in Fig. 11(a) that the transmission spectra are monitored and saved for comparison at different steps. The curvature values are set as 0, 0.8841, 1.5313, 1.9769, 2.7957, 3.4240, 3.9537, 4.4204 m^{-1} , respectively. It is evident that the transmission spectra show slight variations at different bending degrees. To reveal transmission intensity change induced by the bending, the relationship between curvature values and peak intensity at 1543 nm is displayed in Fig. 11(b). Compared to 5 dB variation caused by human breath, the curvature-induced fluctuation of transmission intensity at 1543 nm is much smaller with a value less than 0.353 dB. Thus, the all-fiber sensor based on HCBF can be considered as a curvature-insensitive device for human breath monitoring. The comparisons of overall sensing performances between our sensor and previously reported sensors are shown in Table 1.

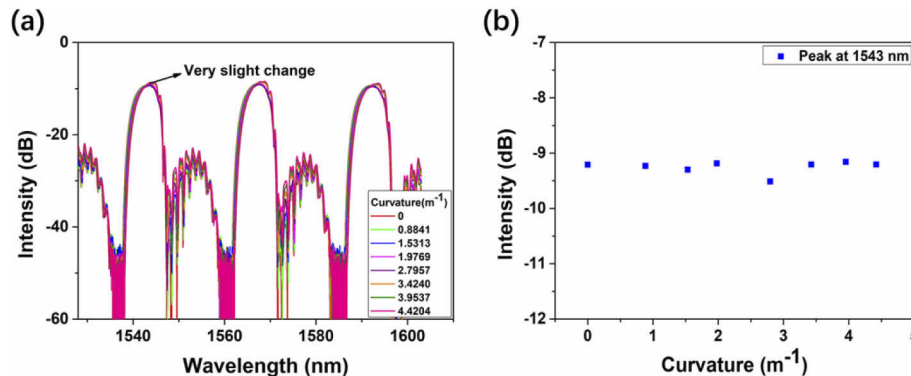


Fig. 11. (a) The transmission spectra of fiber sensor with different curvature values of 0, 0.8841, 1.5313, 1.9769, 2.7957, 3.4240, 3.9537, 4.4204 m^{-1} and (b) the peak intensities statistics at different curvature values

Table 1. Comparison of the key parameters between the proposed all-fiber sensor and other recent-developed fiber-optic sensors in literatures for human breath monitoring

Sensor Structure	Response Time (s)	Recovery Time (s)	Temperature Insensitivity	Curvature Insensitivity
Fiber + hygroscopic polymer [14]	0.5	0.4	Not mentioned	Not mentioned
Fiber + PEO [25]	0.785	Not mentioned	Not mentioned	No
Fiber + MoS ₂ [15]	0.85	0.85	Not mentioned	Not mentioned
Fiber + MoS ₂ [26]	0.066	2.395	Not mentioned	Not mentioned
Fiber + SnO ₂ [16]	0.37	0.37	No	Not mentioned
Fiber + GO [17]	0.042	0.115	No	Not mentioned
Fiber + gelatin [18]	0.084	0.029	Yes	Not mentioned
All-fiber (This work)	0.15	0.65	Yes	Yes

5. Conclusion

An all-fiber sensor based on HCBF has been successfully created in our work which displays excellent performance on human breath monitoring. The response time of the proposed sensor is around 0.15 s which enables the rapid and precise recording of breath signals. The applied distance between the fiber sensor and the human face is also investigated to reveal its influences on sensing results. Moreover, the HCBF sensor proves substantial insensitivity to temperature and curvature variation, which demonstrates its reliable sensing performance in different application environments. The proposed all-fiber sensor has advantages of low price, ease of fabrication, and insensitivity to the change of temperature and curvature, which provides a creative and reliable approach to human breath monitoring.

Funding. Guangdong Provincial Pearl River Talents Program (2017BT01X121); Research Grants Council, University Grants Committee (GRF 15211317).

Acknowledgments. The authors thank the technical support of Shenzhen Research Institute of The Hong Kong Polytechnic University.

Disclosures. The authors declare no conflicts of interest.

Data availability. Data underlying the results presented in this paper are not publicly available at this time but may be obtained from the authors upon reasonable request.

References

1. X. Wen, T. Ning, Y. Bai, C. Li, J. Li, and C. Zhang, "Ultrasensitive temperature fiber sensor based on Fabry-Perot interferometer assisted with iron V-groove," *Opt. Express* **23**(9), 11526–11536 (2015).
2. F. Zhang, X. Xu, J. He, B. Du, and Y. Wang, "Highly sensitive temperature sensor based on a polymer-infiltrated Mach-Zehnder interferometer created in graded index fiber," *Opt. Lett.* **44**(10), 2466–2469 (2019).
3. M. Hernaez, B. Acevedo, A. G. Mayes, and S. Melendi-Espina, "High-performance optical fiber humidity sensor based on lossy mode resonance using a nanostructured polyethylenimine and graphene oxide coating," *Sens. Actuators, B* **286**, 408–414 (2019).
4. W. Yuan, H. Qian, Y. Liu, Z. Wang, and C. Yu, "Highly Sensitive Temperature and Humidity Sensor Based on Carbon Nanotube-Assisted Mismatched Single-Mode Fiber Structure," *Micromachines (Basel)* **10**(2019).
5. S. Dong, B. Dong, C. Yu, and Y. Guo, "High Sensitivity Optical Fiber Curvature Sensor Based on Cascaded Fiber Interferometer," *J. Lightwave Technol.* **36**(4), 1125–1130 (2018).
6. S. Marrujo-Garcia, I. Hernandez-Romano, M. Torres-Cisneros, D. A. May-Arrijoja, V. P. Minkovich, and D. Monzon-Hernandez, "Temperature-independent curvature sensor based on in-fiber Mach-Zehnder interferometer using hollow-core fiber," *J. Lightwave Technol.* **38**(15), 1 (2020).
7. W. Yuan, Q. Zhao, L. Li, Y. Wang, and C. Yu, "Simultaneous measurement of temperature and curvature using ring-core fiber-based Mach-Zehnder interferometer," *Opt. Express* **29**(12), 17915–17925 (2021).
8. M. Quan, J. Tian, and Y. Yao, "Ultra-high sensitivity Fabry-Perot interferometer gas refractive index fiber sensor based on photonic crystal fiber and Vernier effect," *Opt. Lett.* **40**(21), 4891–4894 (2015).
9. W. Yuan and C. Yu, "Dual Demodulation of Temperature and Refractive Index Using Ring Core Fiber Based Mach-Zehnder Interferometer," *Micromachines (Basel)* **12**, 258 (2021).

10. T. Wang, W. Yasukochi, S. Korposh, S. W. James, R. P. Tatam, and S.-W. Lee, "A long period grating optical fiber sensor with nano-assembled porphyrin layers for detecting ammonia gas," *Sens. Actuators, B* **228**, 573–580 (2016).
11. Q. Yao, G. Ren, K. Xu, L. Zhu, H. Khan, M. Mohiuddin, M. W. Khan, B. Y. Zhang, A. Jannat, F. Haque, S. Z. Reza, Y. Wang, X. Wen, A. Mitchell, and J. Z. Ou, "2D Plasmonic Tungsten Oxide Enabled Ultrasensitive Fiber Optics Gas Sensor," *Adv. Opt. Mater.* **7**(24), 1901383 (2019).
12. V. Senwal and B. D. Gupta, "Highly sensitive surface plasmon resonance based fiber optic pH sensor utilizing rGO-Pani nanocomposite prepared by in situ method," *Sens. Actuators, B* **283**, 632–642 (2019).
13. F. Tan, W. Lyu, S. Chen, Z. Liu, and C. Yu, "Contactless vital signs monitoring based on few-mode and multi-core fibers," *Opto-Electron. Adv.* **3**(5), 190034 (2020).
14. S. Akita, H. Sasaki, K. Watanabe, and A. Seki, "A humidity sensor based on a hetero-core optical fiber," *Sens. Actuators, B* **147**(2), 385–391 (2010).
15. D. Li, H. Lu, W. Qiu, J. Dong, H. Guan, W. Zhu, J. Yu, Y. Luo, J. Zhang, and Z. Chen, "Molybdenum disulfide nanosheets deposited on polished optical fiber for humidity sensing and human breath monitoring," *Opt. Express* **25**(23), 28407 (2017).
16. A. Lopez Aldaba, D. Lopez-Torres, C. Elosua, J. L. Auguste, R. Jamier, P. Roy, F. J. Arregui, and M. Lopez-Amo, "SnO₂-MOF-Fabry-Perot optical sensor for relative humidity measurements," *Sens. Actuators, B* **257**, 189–199 (2018).
17. B. Jiang, Z. Bi, Z. Hao, Q. Yuan, D. Feng, K. Zhou, L. Zhang, X. Gan, and J. Zhao, "Graphene oxide-deposited tilted fiber grating for ultrafast humidity sensing and human breath monitoring," *Sens. Actuators, B* **293**, 336–341 (2019).
18. Y. Yi, Y. Jiang, H. Zhao, G. Brambilla, Y. Fan, and P. Wang, "High-Performance Ultrafast Humidity Sensor Based on Microknot Resonator-Assisted Mach-Zehnder for Monitoring Human Breath," *ACS Sens.* **5**(11), 3404–3410 (2020).
19. J. Li, H. Qu, and M. Skorobogatiy, "Squeezed hollow-core photonic Bragg fiber for surface sensing applications," *Opt. Express* **24**(14), 15687–15701 (2016).
20. J. Li, K. Nallappan, H. Guerboukha, and M. Skorobogatiy, "3D printed hollow core terahertz Bragg waveguides with defect layers for surface sensing applications," *Opt. Express* **25**(4), 4126–4144 (2017).
21. J. Li and K. Nallappan, "Optimization of hollow-core photonic Bragg fibers towards practical sensing implementations," *Opt. Mater. Express* **9**(4), 1640–1653 (2019).
22. Y. Wang, G. Yan, Z. Lian, C. Wu, and S. He, "Liquid-level sensing based on a hollow core Bragg fiber," *Opt. Express* **26**(17), 21656–21663 (2018).
23. Z. Liu and H.-Y. Tam, "Fabrication and Sensing Applications of Special Microstructured Optical Fibers," in *Selected Topics on Optical Fiber Technologies and Applications* (2018).
24. Y. Wang, D. Richardson, G. Brambilla, X. Feng, M. Petrovich, M. Ding, and Z. Song, "Intensity Measurement Bend Sensors Based on Periodically Tapered Soft Glass Fibers," *Opt. Lett.* **36**(4), 558–560 (2011).
25. J. Mathew, Y. Semenova, G. Rajan, P. Wang, and G. Farrell, "Improving the sensitivity of a humidity sensor based on fiber bend coated with a hygroscopic coating," *Opt. Laser Technol.* **43**(7), 1301–1305 (2011).
26. B. Du, D. Yang, X. She, Y. Yuan, D. Mao, Y. Jiang, and F. Lu, "MoS₂-based all-fiber humidity sensor for monitoring human breath with fast response and recovery," *Sens. Actuators, B* **251**, 180–184 (2017).